Band offsets and Fermi level pinning at metal-Al$_2$O$_3$ interfaces

Lior Kornblum,[1,*] Jonathan A. Rothschild,[1] Yaron Kauffmann,[1] Reuven Brener,[2] and Moshe Eizenberg[1,2]

[1]*Department of Materials Engineering, Technion–Israel Institute of Technology, Haifa 32000, Israel*
[2]*Solid State Institute, Technion–Israel Institute of Technology, Haifa 32000, Israel*

Disparities between the predicted and the measured effective work functions (EWFs) in advanced metal oxide semiconductor devices, or Fermi-level pinning (FLP), have gained significant attention when high-*k* dielectrics began to emerge. Using a systematic approach for EWF extraction, combined with a comparison to unpinned SiO$_2$ references, it was found that no intrinsic FLP exists in the model dielectric Al$_2$O$_3$. Extrinsic FLP was found with one of the metals investigated Ta, where a 0.4 eV increase in the EWF was observed in the electrical characteristics and confirmed by backside spectroscopy. The physical origins of the band offsets related to the EWF increase have been analyzed in detail. A 2-nm interfacial layer at the Ta-Al$_2$O$_3$ interface has been found and is suggested as the source of extrinsic FLP. Interfacial dipoles originating from Ta-O chemical bonds are considered as the mechanism responsible for the band offset. The results of this model system are then used to explain some of the peculiarities occurring at complex devices which are used in technological applications.

I. INTRODUCTION

Metal-dielectric interfaces have gained increasing interest over the last decade as a result of the challenging integration of high-*k* dielectrics with metal gate electrodes in the microelectronic industry,[1,2] replacing the traditional SiO$_2$/polycrystalline-Si gate stacks. Significant deviations from the expected behavior of devices were found to stem from changes in the band structure[3] of the complex stack that composes the metal oxide semiconductor (MOS) capacitor, which is the heart of an MOS field effect transistor (MOSFET), the building block of modern logic circuitry.

Changes in the band structure and offsets of devices are commonly described with replacement of the expression of the metal's work function (WF) term with an effective WF (EWF), which may include various contributions not related to the pure metal (defined and illustrated in Ref. 3). Theoretical treatment of these WF-EWF deviations is often based on similar discrepancies in the barrier heights of metal-semiconductor (M-S) contacts,[4] which were encountered much earlier. These discrepancies, similarly to the M-S case, are described in terms of Fermi-level pinning (FLP). Explanations to these phenomena range from intrinsic metal-induced interface gap states (MIGS) in the dielectric,[4] intrinsic defects in the dielectric,[5,6] and changes in the dipole at the bottom,[7] middle,[8–10] and top[11–13] of the dielectric stack.

More generally, it was discussed at length whether FLP is caused by an intrinsic mechanism, such as MIGS and later modifications,[14–16] or by extrinsic mechanisms, which are related to other components in the stack. An intrinsic mechanism implies that the FLP is not a function of the metal, while the extrinsic models offer several contributors to FLP, some related to the metal and others to the dielectric and its interfaces. Wen *et al.*[17] have systematically shown that intrinsic factors do not play a role in the case of Hf oxide and Hf silicates as dielectrics. Similar conclusions were obtained by the calculations of Tse *et al.*[13,18]

As metal/high-*k* stacks used for modern devices are only a few nanometers thick and often undergo anneals at temperatures as high as ∼1000 °C, it is extremely difficult to attribute the behavior of the device to a specific phenomenon in a specific region inside the stack. For example, Bosman *et al.* recently reported[19] a thorough chemical analysis of a complex stack with a total (dielectric) thickness of under 5 nm and observed about 2 nm of gradually changing compositions at the metal-dielectric interface. At such overall dimensions and complex stacks, it is hard to evaluate the contribution of a single mechanism to the overall device behavior.

In this work, a simple system was chosen in order to understand the origin and effect of FLP. Al$_2$O$_3$ was chosen as a model dielectric for its simplicity: it is easy to deposit at a fixed stoichiometry; its oxide has a single oxidation state; and unlike Hf-based dielectrics, it is relatively free of oxygen vacancies, which are considered to be one of the causes of FLP.[5,6] The metal side of the system in this work consists of Al and Pt, which are used to establish that there is no intrinsic FLP in the system, and Ta, which serves as a case study of an extrinsic FLP mechanism. In order to make these observations, the contribution of the metal-dielectric interface to the band offsets was systematically separated from other effects. A simple configuration with relatively large device dimensions was intentionally used in order to allow a separation of the contributions unrelated to the metal-dielectric interface.

The materials and configuration of the metal-Al$_2$O$_3$ model system used here are not directly relevant for modern technological applications, but their simplicity allows a better understanding of the physics hidden at the metal-dielectric interface. Moreover, metal-Al$_2$O$_3$ interfaces hold technological relevance in applications, such as ultra-thin capping layers for high-*k* dielectrics,[19,20] for advanced high-mobility channel devices,[21] and blocking layers for modern nonvolatile memories.[22] Of particular interest in the technological context are TaN-Al$_2$O$_3$ stacks,[23–26] which bear some similarities to the Ta-Al$_2$O$_3$ interface hereby investigated.

II. EXPERIMENTAL

First, 50 nm of SiO$_2$ were grown by dry thermal oxidation on a cleaned (100) p-Si wafer: $B \sim 3 \times 10^{15}$ cm^{-3}. The

(a)

Al$_2$O$_3$ over beveled SiO$_2$
EWF extraction

Al$_2$O$_3$ (4.7nm)
SiO$_2$ (15÷50nm)
p-Si

Beveled SiO$_2$
reference for
EWF extraction

SiO$_2$ (15÷50nm)
p-Si

Uniform thickness
C-V analysis

Al$_2$O$_3$ (4.7nm)
SiO$_2$ (7nm)
p-Si

(b)

(c)

(d)
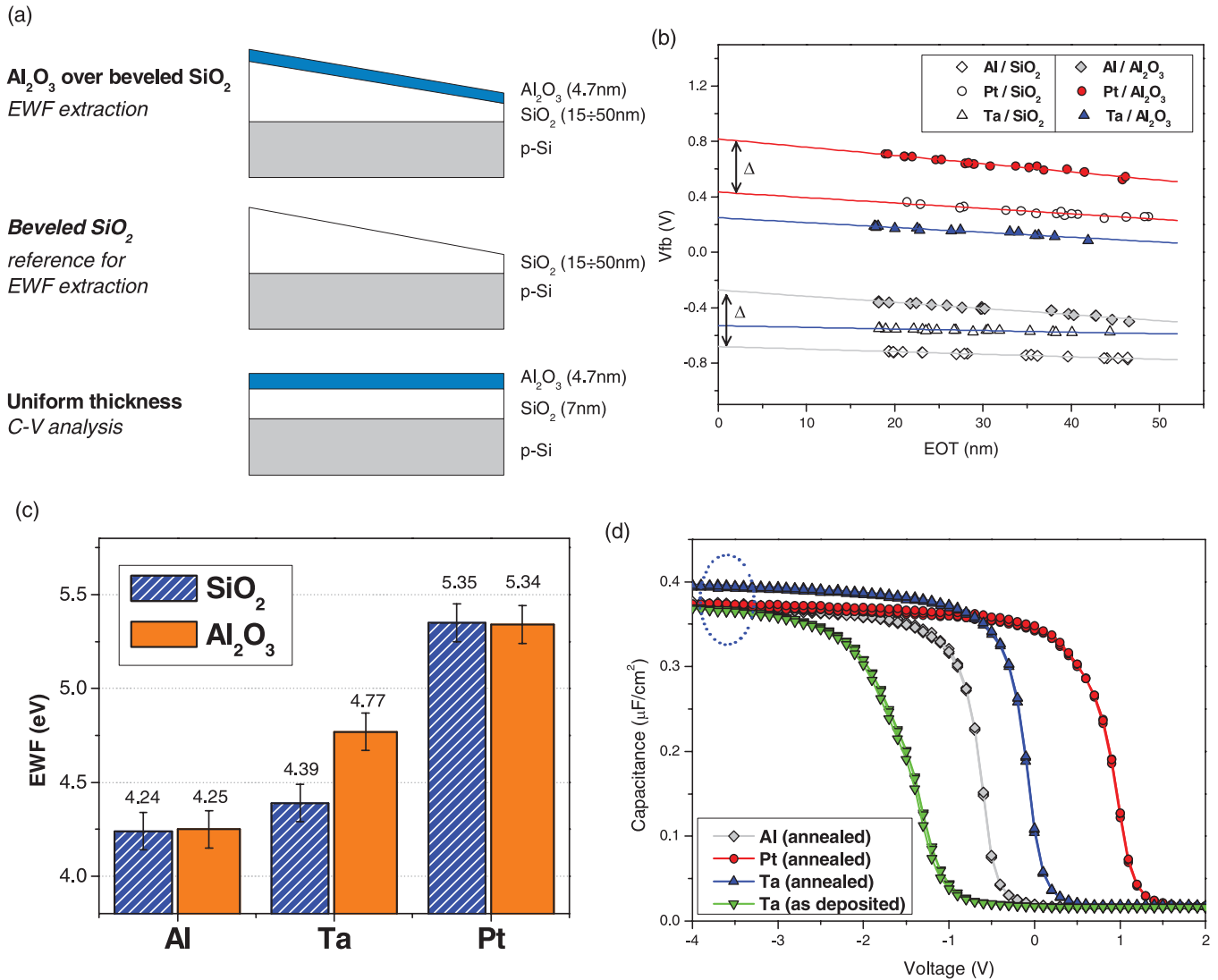
FIG. 1. (Color online) Electrical characteristics of metal-Al$_2$O$_3$ MOS structures: (a) a schematic structure of the different substrates; (b) V_{FB}-EOT plots for EWF extraction of Al, Ta, and Pt on Al$_2$O$_3$ and SiO$_2$ reference; (c) a summary of the EWF values obtained; (d) capacitance-voltage curves of annealed Al, Ta, and Pt samples and an as-deposited Ta sample (uniform thickness structure)

oxide was then gradually etched in a dilute hydrofluoric acid (HF) solution (1:10) to form a beveled structure. Then 4.7 nm of Al$_2$O$_3$ were deposited by atomic layer deposition (ALD) using trimethyl-aluminum and H$_2$O at 300 °C. Metal oxide semiconductor capacitors were formed by room temperature e-beam evaporation of 50 nm of Al, Pt, and Ta through a shadow mask on the following substrates: beveled SiO$_2$ with and without Al$_2$O$_3$, and on a uniform 7-nm SiO$_2$ layer covered with Al$_2$O$_3$ prepared in the same ALD deposition [Fig. 1(a)]. Postmetallization anneal was done in vacuum ($<10^{-7}$ Torr) at 400 °C for 30 min. Cross-section and back-etch specimens were prepared from selected samples.

Capacitance-voltage (C-V) measurements were done in a light-sealed chamber using an HP 4284A LCR meter at 100 KHz. The area of each capacitor was measured using an optical microscope. Transmission electron microscopy in imaging and spectroscopy modes was done using Titan 80-300 scanning/transmission electron microscope (S/TEM, FEI) operated at 300 KeV and equipped with an EDAX

detector (Ametek) for energy-dispersive x-ray spectroscopy (EDX). X-ray photoelectron spectroscopy (XPS, Thermo VG Scientific Sigma Probe) was performed using a monochromatic Al $K\alpha$ (1486.6 eV) source with a pass energy of 30 eV. Line-shape analysis was done using XPSPEAK4.1 software after a Shirley-type background subtraction with a 15% Gaussian–Lorentzian ratio.

To prepare samples for XPS analysis from the backside, layers of Al$_2$O$_3$ deposited by ALD followed by an e-beam deposited Ta layer were fabricated on a clean (100) GaAs wafer under the same conditions and recipes as the other samples of this study. Half of this piece was subjected to a 400 °C anneal at the same conditions as the other samples of this study, and the other half did not undergo any thermal treatment. These samples were then glued from the Ta side to a glass substrate and were etched from the back at room temperature, using a highly selective wet etch that stopped at the Al$_2$O$_3$ layer. The solution used was sulfuric acid, deionized water, and 30% hydrogen peroxide (1:1:8) kept at room temperature.

The relative ease of selective etching is the reason GaAs was chosen for the backside XPS samples.

III. RESULTS AND DISCUSSION

The band structure and offsets of metal-Al_2O_3 MOS structures were investigated using beveled oxide samples [Fig. 1(a)], which allow a systematic and accurate extraction of the EWF, using the intercept of flat-band voltage vs effective oxide thickness (V_{FB}-EOT) plots. Since only the bottom SiO_2 thickness was varied, the general V_{FB} expression[27] can be written as:

$$V_{FB} = \phi_M^{\text{eff}} - \phi_S - \frac{1}{\varepsilon_{ox}} \int_0^{\text{EOT}} x\rho(x)dx, \qquad (1)$$

where ϕ_M^{eff} is the EWF of the specific metal, $\phi_S = k_B T \ln(N_A/n_i) + \chi + E_g/2$ the semiconductor WF (with k_B being Boltzmann's constant, T the absolute temperature, N_A the Si doping, n_i the intrinsic carriers concentration, χ the Si affinity, and E_g its band gap), ε_{ox} the permittivity of SiO_2, x the distance from the metal interface, $\rho(x)$ the charge density, and EOT the equivalent SiO_2 thickness needed to yield the same capacitance.

Assuming that $\rho(x)$ for SiO_2 consists of Si-SiO_2 interface charge, Q_f, and of bulk SiO_2 charge density, ρ_{ox}, simplifies the integration in Eq. (1). To further simplify this expression, the net electrostatic effect of the Al_2O_3 layer is termed Δ. Here, Δ may include bulk Al_2O_3 charges, Al_2O_3-SiO_2 interface charges, or interface dipoles. Whatever its origin, Δ is identical for the various samples since all the Al_2O_3 samples used in this work were prepared in a single ALD process. Equation (1) can now be written as:

$$V_{FB} = \phi_M^{\text{eff}} - \phi_S - \left(\frac{Q_f}{\varepsilon_{ox}}\text{EOT} + \frac{1}{2}\frac{\rho_{ox}}{\varepsilon_{ox}}\text{EOT}^2 \right) + \Delta. \qquad (2)$$

Extraction of the metal EWF using V_{FB}-EOT plots is shown in Fig. 1(b) for Al, Ta, and Pt on Al_2O_3 and on SiO_2, which is used as a reference. To simplify the nomenclature, all samples are annealed unless specifically noted otherwise. The agreement of these plots to the linear fits indicates $Q_f \gg \rho_{ox} \cdot \text{EOT}/2$, namely the cubic term of Eq. (2) is negligible, which is common for high-quality thermal SiO_2. The differences in intercept between the Al_2O_3 sample and the SiO_2 reference for Al and Pt yield $\Delta = 0.4$ eV. Adding an Al_2O_3 dielectric is known to increase the EWF, and this property is in fact exploited for EWF control using ultrathin dielectric capping layers. Effective work function increase of 0.2–0.4,[28] 0.57,[29] and 0.6 eV[30] were reported following an addition of Al_2O_3 with different configurations, similar in magnitude and direction to Δ. In addition, Coss *et al.*[31] measured a 0.3–0.5 eV decrease in the Schottky barrier height (SBH) on p-Si following an insertion of Al_2O_3, which is another way of expressing a similar increase in the EWF over p-Si. The EWF can now be extracted after subtraction of Δ and $\phi_S = 4.92$ eV (extracted from the C-V curves[27]) from the intercepts of the V_{FB}-EOT plots [Fig. 1(b)]. The summary of the EWF values [Fig. 1(c)] indicates that no intrinsic FLP exists in the system, according to the excellent agreement of the EWF of Al and Pt on Al_2O_3 vs the unpinned SiO_2 reference. This extends what was calculated[13,18] and measured[17] with HfO_2

and $HfSiO_x$ to Al_2O_3. Moreover, Fig. 1(c) clearly shows an increase of 0.38 ± 0.1 eV in the EWF of Ta on Al_2O_3, which implies an extrinsic, metal-dependent FLP. In other words, a different band offset is observed, which can also be expressed as a different SBH in the Ta-Al_2O_3 sample.

The first hint of an extrinsic FLP mechanism can be seen in the comparison between the capacitance-voltage (C-V) behavior of samples deposited on a uniform thickness dielectric stack [Fig. 1(a)]. Figure 1(d) presents C-V curves of annealed Al, Ta, and Pt capacitors, and as-deposited (i.e. not annealed) Ta capacitors. Each curve in Fig. 1(d) is composed of measurements of three different capacitors that overlap. The annealed Ta curves show an increase in capacitance in the accumulation region with respect to the others. In the accumulation region, the MOS capacitance is expressed as a simple plate capacitor:

$$\frac{C_{\text{acc}}}{A} = \frac{k\varepsilon_0}{t} = \frac{\varepsilon_{ox}}{\text{EOT}}, \qquad (3)$$

where C_{acc} is the accumulation capacitance, A the area, k the relative dielectric constant, ε_0 the vacuum permittivity, and t the dielectric thickness.

Measurements of the Ta sample prior to the 400 °C anneal yield capacitance values similar to those of Al and Pt, which indicates that the observed capacitance increase is a result of the anneal. As the areas are measured specifically for each capacitor, an increase in C_{acc} cannot be explained by an additional series capacitor, and it can only stem from a reduction in the EOT, an increase of k, or a combination of both [Eq. (3)]. Note that the large negative V_{FB} value of the as-deposited Ta curve is originated in e-beam-induced charging of the dielectric during deposition, which is known to be removed during anneal. Based on this change in capacitance, it is hypothesized that the extrinsic FLP mechanism is activated during anneal.

In order to get to the bottom of the physical origin of this band offset at the Ta-Al_2O_3 sample, XPS spectra were collected from back-etched samples. Al 2p and Ta 4f spectra taken from as-deposited and annealed samples are compared in Fig. 2. Charging compensation is done by horizontally aligning the Al 2p peaks of both spectra [Fig. 2(a)] to 74.3 eV. The Ta 4f spectra of both samples [Fig. 2(b)] consist of a major metallic Ta 4f doublet at low binding energies (BE), three partially oxidized Ta 4f doublets, and a small O 2s contribution.[32] The overall shape of these peaks corresponds well to a Ta suboxide on metallic Ta (Refs. 33 and 34).

The most noteworthy feature of Fig. 2(b) is the clear shift of the metallic component of Ta to a higher BE as a result of the annealing step. This shift, quantified as 0.44 ± 0.05 eV by the deconvoluted metallic Ta peak, cannot be explained by charging of the sample since the Al 2p peaks are aligned. As bulk Ta does not change during a 400 °C anneal, the only remaining explanation to the observed shift is the formation of a dipole layer between the Al_2O_3 layer and the metallic Ta, pointing from the metal to the dielectric. This dipole layer corresponds well both in direction and in magnitude to the 0.38 ± 0.1 EWF shift observed in the electrical measurements [Fig. 1(c)]. This outcome that an increase of the metallic Ta BE is similar to an increase of the Ta EWF is expected since both increases represent a larger energetic distance from the
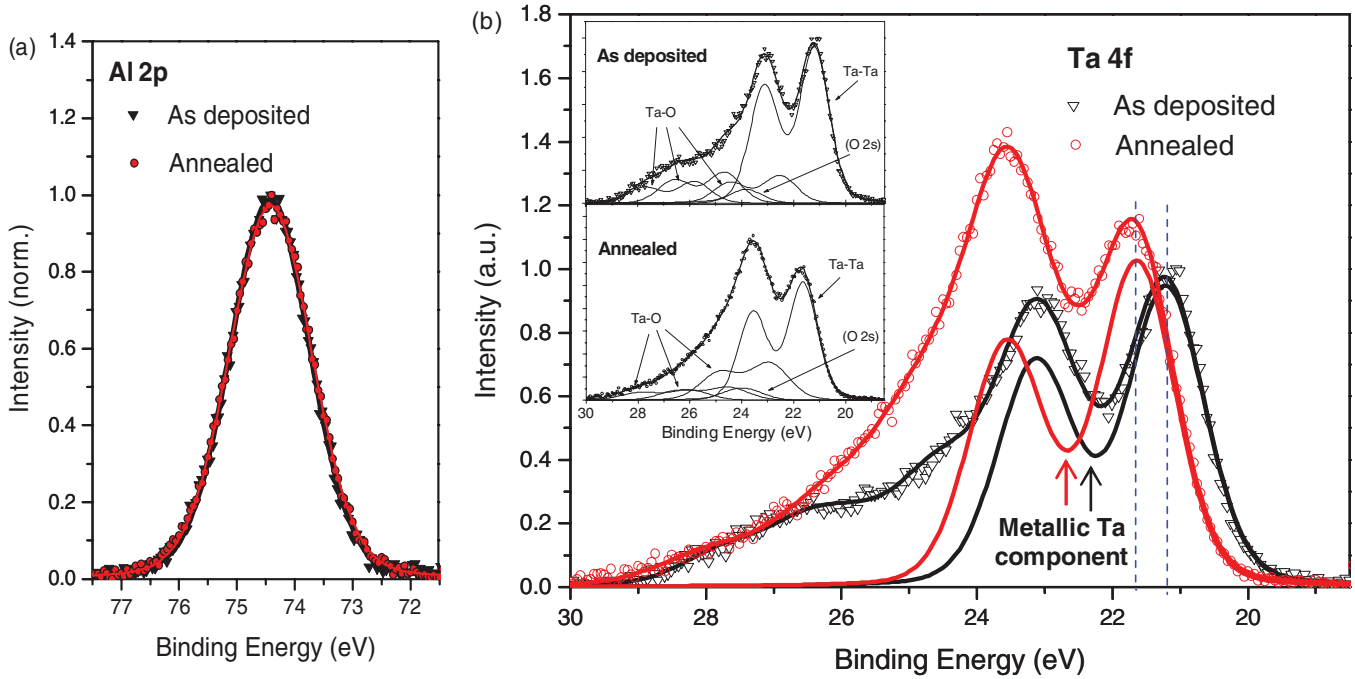
FIG. 2. (Color online) XPS spectra of (a) Al 2*p* and (b) Ta 4*f* taken from the back of annealed and as-deposited samples and normalized by the maximum Al 2*p* intensity. Inset shows the deconvoluted components of Ta 4*f*.

vacuum level of electrons at a core level (4f, XPS) or the Fermi level (EWF).

In order to probe the mechanism responsible for the observed band offset, cross-sectional high-resolution scanning transmission electron microscopy (STEM) micrographs of the Ta-Al$_2$O$_3$ interface were taken [Fig. 3(a)] using a high-angle annular dark field (HAADF) detector. These images clearly show the formation of a ∼2-nm layer at the annealed Ta-Al$_2$O$_3$

interface. The presence of Si lattice fringes in Fig. 3(a) confirms that the sample is edge on with respect to the beam, and the spatial resolution is well below 0.4 nm, validating that the observed interface layer (IL) is not an imaging artifact.

The results so far suggest that the IL may be responsible for the measured band offset at the Ta-Al$_2$O$_3$ interface. In order to understand the effect of this nanometric layer on
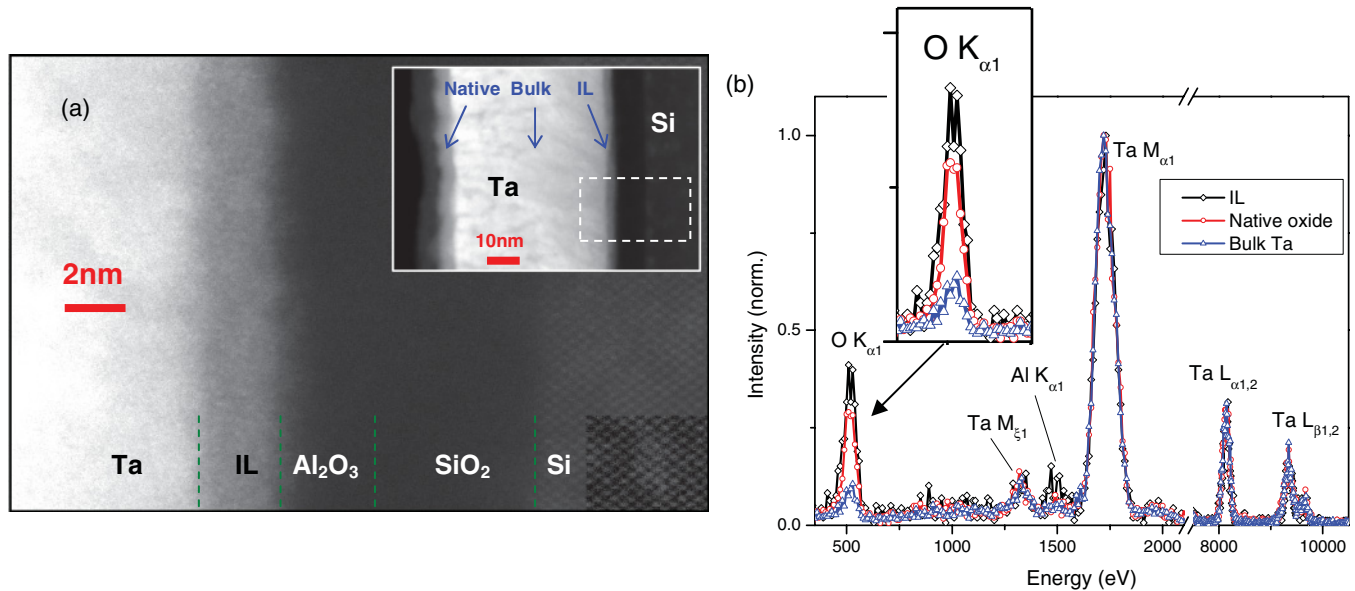
FIG. 3. (Color online) (a) HAADF-STEM cross-section micrograph of an annealed Ta/Al$_2$O$_3$/SiO$_2$/Si sample. The bottom right corner is shown at a different brightness to emphasize the lattice fringes. Inset shows the interface at a lower magnification with a dashed rectangle representing the borders of the larger image. (b) Normalized EDX spectra taken from different regions as illustrated in (a), with the inset showing a close-up on the O K$_{\alpha 1}$ peak.

the macroscopic device properties, the layer's origin and properties should be addressed.

The mechanism behind the IL formation is a reaction between Ta and Al_2O_3 during anneal, which results in a layer of mixed Ta, Al, and O, and consequently a decrease in the Al_2O_3 thickness. Prior to further characterization and analysis of this layer, a more basic question needs to be addressed: is the Ta-Al_2O_3 interface stable, and could such a reaction be thermodynamically justified? Assuming the reaction is driven by the reduction of Al_2O_3 by Ta, it can be written per mole of Al_2O_3 as:

$$Al_2O_3 + x \cdot Ta \rightarrow Al_y Ta_x O_3 + (2 - y) \cdot Al. \qquad (4)$$
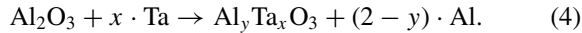
The phase diagram suggests[35] that $AlTaO_4$ is the stable phase, with possibilities of $Al_7Ta_3O_{18}$ and $AlTa_9O_{24}$ as well. As no thermodynamic parameters are known for these phases, the more simple case of Al_2O_3 reduction will be considered. When written per mole of O and for $y = 0$, Eq. (4) becomes:

$$\tfrac{1}{3}Al_2O_3 + \tfrac{2}{5}Ta \rightarrow \tfrac{1}{5}Ta_2O_5 + \tfrac{2}{3}Al. \qquad (5)$$
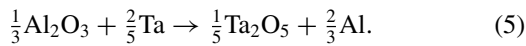
Assuming the formation entropies and enthalpies do not considerably change in the 300–673 K range, and using $\Delta G = \Delta H - T\Delta S$ we obtain[36] $\Delta G \cong -9.2 \times 10^3$ kJ × mol^{-1}. This value serves as a very rough indication that the Ta-Al_2O_3 interface is unstable at $400\,^\circ$C. Although the system is far away from equilibrium, thermodynamics may provide a general qualitative direction at which the system will evolve. Moreover, in the case of the more stable TaN-Al_2O_3 interface, Al_2O_3 reduction was observed[23] above $700\,^\circ$C. This may further imply that metallic Ta, which is known for its affinity to oxygen, may promote Al_2O_3 reduction at even lower temperatures.

In order to evaluate the O:Ta ratio in the different regions, EDX spectra were acquired from different regions of the sample [inset of Fig. 3(a)]. The spectra are shown in Fig. 3(b), with the intensities normalized with respect to the Ta $M_{\alpha 1}$ peak. The top surface of the metal is used as a standard assuming it is Ta_2O_5, the only stable oxidation state of Ta, marked as native in Fig. 3(a). The normalized spectra therefore indicate that the IL layer possesses an O:Ta ratio higher than that of the native oxide. This is reasonable because the IL also contains Al [seen in Fig. 3(b)] that is bound to O as well.

More on the chemical nature of the interface can be deduced from the inset of Fig. 2(b), where an increase in the nonmetallic components of the Ta spectrum is seen after anneal. If the relative oxidation is schematically defined as the ratio between the area of the oxidized Ta doublets to the total area of the spectrum, it can be shown that this value increases by about 30% following anneal (the O 2s contribution is neglected for this estimation, as it constitutes less than 5% of the total area). Since the XPS signal depth is shallow ($<$10 nm) and the metallic Ta signal does not change considerably, the increased oxide component suggests that partially oxidized Ta infiltrated the Al_2O_3 layer.

Combining the increase in the capacitance of the Ta samples [Fig. 1(d)] with the microscopy and spectroscopy results, we conclude that Ta reacts with Al_2O_3 and in doing so infiltrates the latter to about 2 nm from the original interface. We further recall that almost no Ta_2O_5 signal is observed in XPS

[Fig. 2(b)], indicating that the IL is composed of partially oxidized Ta in Al_2O_3. This means that $\sim$2 nm of Al_2O_3 are replaced by the IL, which has a higher dielectric constant, thus accounting for the increased capacitance. The reduced Al most probably dissolves in the metallic Ta, again with similarities to observations made on the TaN-Al_2O_3 system.[23] If we assume that the total dielectric thickness does not change considerably, and use k values separately extracted for the Al_2O_3 used here, we obtain $k \approx 18$ for the IL. This value is close to the range of values obtained for Ta_2O_5:Al_2O_3 mixtures previously reported,[37,38] although it is important to note that the Ta is not fully oxidized in this case.

It has previously been shown that metals such as Hf and Ti can scavenge oxygen from the bottom part of the dielectric stack, which results in a capacitance increase and shifts in the band offsets of devices.[7,39,40] However, this effect cannot explain the results reported here, since the Ta on the SiO_2 reference sample does not exhibit a capacitance increase (not shown here). Moreover, there is a distinct difference between the EWF of Ta on Al_2O_3 and Ta on SiO_2, with the latter in agreement the vacuum WF of Ta, 4.25 eV.[36] Therefore, the band offsets of annealed Ta-Al_2O_3 can only be attributed to the IL formation.

Having accounted for the increased capacitance with the IL formation, we will now explain how it can increase the EWF by changing the band offset at the metal-dielectric interface. First, polarized chemical bonds at the interface are considered as the origin of the band offset. Ta-O bonds with preferred directionality are abundant at the interface between the metallic Ta and the O-rich IL. These bonds create a dipole layer pointing from the metal to the dielectric [Fig. 4(a), top], which causes band offsets in the proper direction to account for the increase in the EWF. To estimate the required density of Ta-O chemical bond dipoles needed to account for the measured 0.4-eV band offset, a simple electrostatic calculation[41] is employed:

$$N = \frac{\Delta EWF}{\delta} \cdot \frac{\varepsilon_0}{q^2} \cdot \left\{ 1 - \exp\left[-\left(\frac{\chi_{Ta} - \chi_O}{2} \right)^2 \right] \right\}^{-1}, \quad (6)$$

where N is the surface dipoles density, $\delta \approx 1.7$ A the dipole length,[42] and χ_{Ta} and χ_O the Pauling electronegativities of Ta and O, respectively.

Using Eq. (6) yields $\sim$2 $\times$ 10^{13} cm^{-2}, which is two orders of magnitude smaller than the surface density of atoms in metallic Ta. It is possible that the actual density is higher, but depolarization causes a reduction in the overall potential drop.[43] Therefore, polarized chemical bonds may be attributed to the observed band offset, as only a few percents of the interface atoms are needed to create such dipoles in order to account for the observed phenomenon. It can be argued that if polarized chemical bonds cause the band offset, it should occur not only at Ta-Al_2O_3 interfaces, but also at Ta-SiO_2, Al-SiO_2 and Al-Al_2O_3 interfaces, since Al has an electronegativity value similar to that of Ta. However, the Ta-Al_2O_3 differs by the IL formation, where the O atoms are not in the same chemical state as they are in stoichiometric SiO_2 or Al_2O_3. These O atoms may form chemical bonds and dipoles more readily than in the case of stoichiometric dielectrics. Moreover, due to the above-discussed reaction, the Ta-IL interface has a more
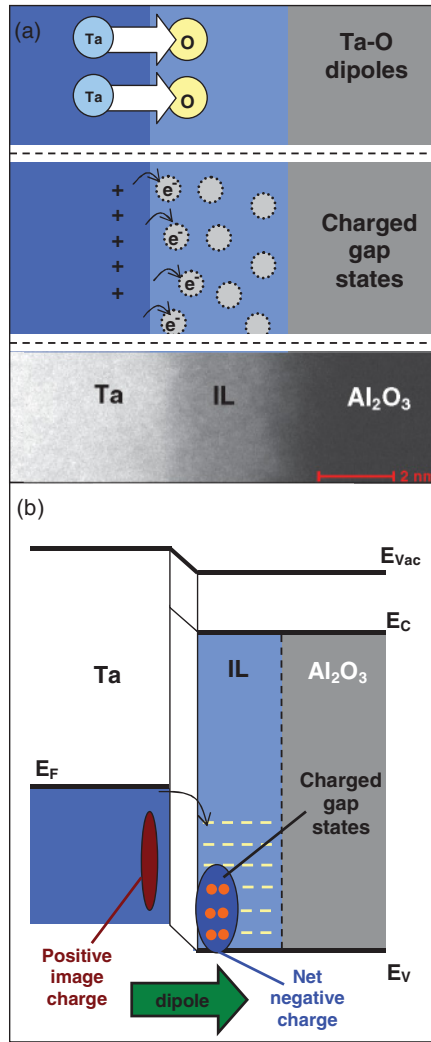
FIG. 4. (Color online) (a) Schematic illustration of chemical dipoles (top), charged gap states (middle), and STEM image (bottom). (b) Schematic band structure showing the dipole formation due to charged gap states.

intimate contact between the metal and the dielectric, which may enhance the formation of the dipoles that are formed.

Alternatively, the infiltrated Ta atoms in the IL may have additional effects other than increasing k. One of these effects can involve the formation of electronic states in the band gap of the IL. The states close enough to the metal can be charged with electrons, creating a negative surface charge [Fig. 4(a), middle]. This charge will cause positive image charges to accumulate in the metal side of the Ta-IL interface, thus producing a dipole layer pointing at the direction measured by EWF and by XPS [Fig. 4(b)]. Most of the many theoretical and experimental works on impurities in Al_2O_3 deal with crystalline phases, and no works dealing with Ta in Al_2O_3 were found. However, such states were reported for V and Nb implanted in amorphous Al_2O_3 (Ref. 44) and for Nb and Zr grown inside amorphous Al_2O_3 (Ref. 45).

When re-examining the experimental results, the dipole model emerges as the better candidate to account for the observed behavior. Collection of XPS spectra is based on ionization of electrons from the sample, which are com-

pensated by electrons flooded by a low-energy gun.[46] If charged or partially charged states in the IL are responsible for the band offset, it is unlikely that the states will be repopulated during the measurement in the same manner they were populated before the measurement. The width of the deconvoluted features of Fig. 2(b) does not show any change following anneal. Therefore, it is not expected that the charged states model will enable to measure the band offset by XPS [Fig. 2(b)], while obtaining the same shift as observed from the EWF [Fig. 1(c)].

IV. SUMMARY AND CONCLUSIONS

Metal-Al_2O_3 interfaces were investigated and revealed that Al and Pt show the same electrical behavior as on the unpinned SiO_2 reference samples, indicating that intrinsic FLP does not occur on Al_2O_3. Furthermore, an unexpected band offset was observed in the case of Ta-Al_2O_3, indicating an extrinsic FLP. The band offset measured from the EWF is found to be in good agreement with the band offset measured by XPS taken from the backside. The observed band offset is traced to the formation of an IL, which is analyzed and found to be the outcome of a reaction between Ta and Al_2O_3. Two possibilities are suggested for the mechanism by which the IL causes the band offsets: dipoles at the metal-dielectric interface or charged defects in the IL side of the Ta-IL interface. Further consideration renders the latter mechanism less likely due to the expected instability of states population during the XPS measurements used to characterize the band offsets. We thus conclude that dipoles from Ta-O bonds at the Ta-IL interface are the mechanism causing extrinsic FLP in the unpinned metal-Al_2O_3 system.

It is noteworthy that the more technologically relevant system of TaN-Al_2O_3 is far more thermally stable.[23] However, many of these stacks and devices undergo an aggressive thermal treatment at $\sim 1000\,^\circ C$, which may form nonabrupt metal-dielectric interfaces as observed for the TiN-Al_2O_3 system.[19] Similar reactions[23] can be the extrinsic cause for band offsets at such systems. Moreover, Al_2O_3 is used as a dielectric capping layer since it is known to increase the EWF, which is attributed to dipoles unrelated with the metal.[10] However, in this paper, the high-k contribution unrelated to the metal (Δ) was of the same magnitude as that of the metal-dielectric interface. Therefore, the results brought here suggest an alternative mechanism for this behavior. This implies that for certain MOS configurations and process conditions, the metal-dielectric interface may be the dominant factor in the overall band structure of various devices.

*Corresponding author. liork@technion.ac.il

[1] G. D. Wilk, R. M. Wallace, and J. M. Anthony, J. Appl. Phys. **89**, 5243 (2001).

[2] J. Robertson, Rep. Prog. Phys. **69**, 327 (2006).

[3] J. Robertson, J. Vac. Sci. Technol. B **27**, 277 (2009).

[4] Y. C. Yeo, T. J. King, and C. Hu, J. Appl. Phys. **92**, 7266 (2002).

[5] S. Guha and V. Narayanan, Phys. Rev. Lett. **98**, 196101 (2007).

[6] O. Sharia, K. Y. Tse, J. Robertson, and A. A. Demkov, Phys. Rev. B **79**, 125305 (2009).

[7] C. Choi and J. C. Lee, J. Appl. Phys. **108**, 064107 (2010).

[8] Z. C. Yang, A. P. Huang, L. Yan, Z. S. Xiao, X. W. Zhang, P. K. Chu, and W. W. Wang, Appl. Phys. Lett. **94**, 252905 (2009).

[9] O. Sharia, A. A. Demkov, G. Bersuker, and B. H. Lee, Phys. Rev. B **77**, 085326 (2008).

[10] P. D. Kirsch, P. Sivasubramani, J. Huang, C. D. Young, M. A. Quevedo-Lopez, H. C. Wen, H. Alshareef, K. Choi, C. S. Park, K. Freeman, M. M. Hussain, G. Bersuker, H. R. Harris, P. Majhi, R. Choi, P. Lysaght, B. H. Lee, H. H. Tseng, R. Jammy, T. S. Böscke, D. J. Lichtenwalner, J. S. Jur, and A. I. Kingon, Appl. Phys. Lett. **92**, 092901 (2008).

[11] K. Xiong, J. Robertson, G. Pourtois, J. Pétry, and M. Müller, J. Appl. Phys. **104**, 074501 (2008).

[12] Y. Kita, S. Yoshida, T. Hosoi, T. Shimura, K. Shiraishi, Y. Nara, K. Yamada, and H. Watanabe, Appl. Phys. Lett. **94**, 122905 (2009).

[13] K. Y. Tse, D. Liu, and J. Robertson, Phys. Rev. B **81**, 035325 (2010).

[14] V. Heine, Phys. Rev. **138**, A1689 (1965).

[15] A. M. Cowley and S. M. Sze, J. Appl. Phys. **36**, 3212 (1965).

[16] W. Mönch, Phys. Rev. Lett. **58**, 1260 (1987).

[17] H. Wen, P. Majhi, K. Choi, C. Park, H. Alshareef, H. Rustyharris, H. Luan, H. Niimi, H. Park, and G. Bersuker, Microelectron. Eng. **85**, 2 (2008).

[18] K. Y. Tse and J. Robertson, Phys. Rev. Lett. **99**, 086805 (2007).

[19] M. Bosman, Y. Zhang, C. K. Cheng, X. Li, X. Wu, K. L. Pey, C. T. Lin, Y. W. Chen, S. H. Hsu, and C. H. Hsu, Appl. Phys. Lett. **97**, 103504 (2010).

[20] L. Hong-Jyh and M. I. Gardner, IEEE Electron Device Lett. **26**, 441 (2005).

[21] E. J. Kim, E. Chagarov, J. l. Cagnon, Y. Yuan, A. C. Kummel, P. M. Asbeck, S. Stemmer, K. C. Saraswat, and P. C. McIntyre, J. Appl. Phys. **106**, 124508 (2009).

[22] M. Lisiansky, A. Heiman, M. Kovler, A. Fenigstein, Y. Roizin, I. Levin, A. Gladkikh, M. Oksman, R. Edrei, A. Hoffman, Y. Shnieder, and T. Claasen, Appl. Phys. Lett. **89**, 153506 (2006).

[23] J. Kwon and Y. J. Chabal, Appl. Phys. Lett. **96**, 151907 (2010).

[24] C. H. Lee, K. C. Park, and K. Kim, Appl. Phys. Lett. **87**, 073510 (2005).

[25] L. Guo-Qiang, Z. Chunxiang, J. Fu, K. Dim-Lee, and N. Singh, IEEE Electron Device Lett. **30**, 662 (2009).

[26] Y. T. Chen, H. Zhao, J. H. Yum, Y. Wang, F. Xue, F. Zhou, and J. C. Lee, Appl. Phys. Lett. **95**, 013501 (2009).

[27] E. H. Nicollian and J. R. Brews, *MOS (Metal Oxide Semiconductor) Physics and Technology* (Wiley, New York, 1982), Chap. 10, pp. 423–491.

[28] Y. Kamimuta, K. Iwamoto, Y. Nunoshige, A. Hirano, W. Mizubayashi, Y. Watanabe, S. Migita, A. Ogawa, H. Ota, T. Nabatame, and A. Toriumi, *Tech. Digest IEDM* (IEEE, Washington DC, 2007), p. 342.

[29] K. Iwamoto, A. Ogawa, Y. Kamimuta, Y. Watanabe, W. Mizubayashi, S. Migita, Y. Morita, M. Takahashi, H. Ito, H. Ota, T. Nabatame, and A. Toriumi, *Symp. on VLSI Tech. Digest* (IEEE, Kyoto, Japan, 2007), p. 70.

[30] K. Choi, H. C. Wen, G. Bersuker, R. Harris, and B. H. Lee, Appl. Phys. Lett. **93**, 133506 (2008).

[31] B. E. Coss, W. Y. Loh, R. M. Wallace, J. Kim, P. Majhi, and R. Jammy, Appl. Phys. Lett. **95**, 222105 (2009).

[32] To simplify the analysis, the metallic component of Ta 4*f* was fitted with a symmetric peak. It should be noted that the metallic component has the lowest BE in the spectra. Therefore, the shift in this component is identical to the overall shift of the entire spectra. Using an asymmetric fit may diminish the small O 2*s* peak or change the ratio between the oxidized Ta 4*f* components. Such changes have no effect on the results and discussion in this work.

[33] S. F. Ho, S. Contarini, and J. W. Rabalais, J. Phys. Chem. **91**, 4779 (1987).

[34] M. Khanuja, H. Sharma, B. Mehta, and S. Shivaprasad, J. Electron Spectrosc. **169**, 41 (2009).

[35] B. W. King, J. Schultz, E. A. Durbin, W. H. Duckworth, US Atomic Energy Commission Report BMI-1106, 1 (1956).

[36] *CRC Handbook of Chemistry and Physics*, 60th ed., edited by R. C. Weast (CRC, Boca Raton, FL, 1980), pp. D67–D76.

[37] C. S. Desu, P. C. Joshi, and S. B. Desu, J. Electroceramics **10**, 209 (2003).

[38] Y. Ezhovskii and A. Klusevich, Phys. Solid State **45**, 2203 (2003).

[39] H. Kim, P. C. McIntyre, C. On Chui, K. C. Saraswat, and S. Stemmer, J. Appl. Phys. **96**, 3467 (2004).

[40] K. I. Seo, D. I. Lee, P. Pianetta, H. Kim, K. C. Saraswat, and P. C. McIntyre, Appl. Phys. Lett. **89**, 142912 (2006).

[41] L. Pauling, *The Nature of the Chemical Bond and the Structure of Molecules and Crystals: An Introduction to Modern Structural Chemistry*. (Cornell University Press, Ithaca, New York, 1960).

[42] W. Zheng, X. Li, S. Eustis, and K. Bowen, Chem. Phys. Lett. **460**, 68 (2008).

[43] W. Mönch, *Semiconductor Surfaces and Interfaces* (Springer, Berlin, 2001), Chap. 14.7, pp. 307–309.

[44] M. C. Kim, S. H. Hong, H. R. Kim, S. Kim, S.-H. Choi, R. G. Elliman, and S. P. Russo, Appl. Phys. Lett. **94**, 112110 (2009).

[45] R. Jung, J. C. Lee, Y. W. So, T. W. Noh, S. J. Oh, J. C. Lee, and H. J. Shin, Appl. Phys. Lett. **83**, 5226 (2003).

[46] J. C. Vickerman, *Surface Analysis: The Principal Techniques* (John Wiley, Chichester, UK, 1997), Chap. 3.5, p. 55–56.